



# 1 Intensified upwelling: normalized sea surface temperature trends 2 expose climate change in coastal areas

3 Miguel Ángel Gutierrez-Guerra<sup>1,2</sup>, María Dolores Pérez-Hernández<sup>1</sup>, Pedro Vélez-Belchí<sup>2</sup>

4 <sup>1</sup> Unidad Océano y Clima, Instituto de Oceanografía y Cambio Global, IOCAG, Universidad de Las Palmas de Gran Canaria,  
5 ULPGC, Unidad Asociada ULPGC-CSIC, Canary Islands, Spain

6 <sup>2</sup> Centro Oceanográfico de Canarias, Instituto Español de Oceanografía, Santa Cruz de Tenerife, Canary Islands, Spain  
7 *Corresponding author:* Miguel A. Gutierrez-Guerra, miguel.gutierrez104@alu.ulpgc.es

## 8 9 **Abstract.**

10 The Eastern Boundary Upwelling Systems (EBUS) provide valuable natural resources due to their high primary production.  
11 However, there is significant uncertainty in how climate change may affect the mechanisms that sustain these ecosystems in  
12 the future. Therefore, assessing the effects of climate change on the EBUS under the current global warming scenario is crucial  
13 for efficient ecosystem management. In 1990, Andrew Bakun suggested an increase in the upwelling intensity due to the rise  
14 of the ocean-land pressure gradient. Since there is a significant link between thermal gradients and offshore Ekman transport,  
15 we use deseasonalized sea surface temperature (SST) data from remote sensing to elucidate this hypothesis and validate it  
16 using in-situ observations. SST is an indicator of coastal upwelling, and our long-term analysis of monthly and deseasonalized  
17 SST records shows that the seasonal and synoptic processes have minimal influence on the SST-upwelling intensity  
18 relationship. Upwelling within the same EBUS is not usually evenly distributed along coastlines, leading to upwelling in  
19 specific areas, upwelling centers. We compare the SST trends in the main upwelling centers of the four EBUS with those in  
20 open ocean waters through a new index,  $\alpha_{UI}$ , designed to characterize upwelling changes in the EBUS. An adimensional  
21 number allows us to normalize the trends independently of the upwelling system and compare all of them. This new index  
22 indicates intensification in all the EBUS, revealing a coherent pattern within EBUS in the same ocean (i.e., Canarian and  
23 Benguela or Californian and Humboldt Upwelling Systems).

## 24 **1. Introduction**

25 The world's major coastal upwelling areas exist along the eastern margins of the Pacific and the Atlantic Oceans. These  
26 extended coastal upwelling systems are known as Eastern Boundary Upwelling Systems (EBUS) and sustain the most  
27 important fisheries in the world (Pauly and Christensen, 1995). The rise of cool, nutrient-rich waters supports the high primary  
28 production needed to maintain these complex ecosystems (Ekman, 1905). Their economic and ecological relevance explains  
29 the association of the EBUS with the world's major Large Marine Ecosystems (LME) (Fig 1). LME are a globalized approach  
30 to a management framework that defines and ranks marine regions based on their gross primary production (Sherman and  
31 Hempel, 2008), and four of the largest LME are embedded in the EBUS worldwide (Kämpf and Chapman, 2016).



32 Bakun, (1990) hypothesized that the sea-land temperature gradient will increase under climate change and therefore, it should  
33 increase the upwelling intensity. The hypothesized increase in the temperature gradient arises from an increased atmospheric  
34 pressure gradient between the low-pressure cell that develops over the heated land mass and the high-pressure cell existing  
35 over the colder ocean. Therefore, as the land warms faster than the ocean, it enhances the low-pressure cells. Thus, the increase  
36 in the pressure gradient drives more intense upwelling favorable winds, intensifying the cold imprint in the Sea Surface  
37 Temperature (SST) near the shore. However, previous studies that have tested Bakun's hypothesis with in-situ data have found  
38 contradictory long-term trends (Barton et al., 2013; Belkin, 2009; McGregor et al., 2007; Rykaczewski et al., 2015; Sambe et  
39 al., 2016)

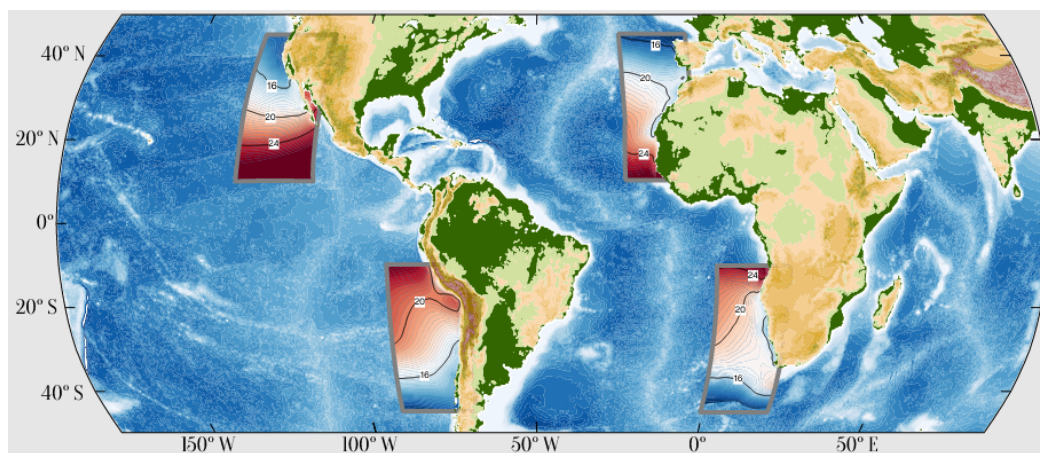


**Figure 1: Location of the EBUS (colored areas) in the world, associated with eastern boundary currents. For each region, the enclosed area includes the mean SST from 1982-2022.**

40 Sydeman et al., (2014) performed a meta-analysis of 18 trends obtained from independent studies of wind stress, both from  
41 observational and model data. Observational data were more likely to report an increase in wind stress in the four EBUS than  
42 model data (excluding Benguela, where no observations were considered). However, the model data were less consistent  
43 between EBUS, showing agreement with observations only in the case of the California system (both supporting  
44 intensification) and for the Iberian system (with a consistent weakening of the wind stress). García-Reyes et al., (2015) also  
45 remarked that in climate change models, the upwelling-related cooling trends were difficult to reproduce due to the small  
46 spatial scale of the coastal upwelling process. Such a controversy between the model, and different observations reflects the  
47 complexity of EBUS dynamics.

48 Upwelling within the same EBUS is not usually evenly distributed along coastlines because of irregular coastlines and  
49 seafloors, leading to more pronounced upwelling in specific areas known as 'upwelling centers' (Kämpf and Chapman, 2016).  
50 These centers are characterized by strong frontal areas and upwelling jets that create eddies. In these areas, the sea surface  
51 temperature drops due to the upwelling of cold subsurface water. Therefore, the relationship between sea surface  
52 (SST) and the upwelling intensity is more robust in these upwelling centers. Even in cases where a generalized increase in



53 favorable upwelling winds occurs, the appearance of cold SST cores, associated with increased upwelling intensity, remains  
54 predominantly confined to these specific areas. Therefore, to study the long-term changes in the upwelling, a good approach  
55 is to focus on these representative upwelling areas within the EBUS since they show a higher signal-to-noise ratio between the  
56 SST and Ekman transport.

57 The main motivation of this study is to assess the impacts of climate change on the four EBUS. This is pursued by using  
58 satellite-derived SST trends as a proxy for changes and a new index that normalizes the upwelling trend of the coastal upwelling  
59 with the oceanic background trends. Specifically, we have chosen points representative of each dynamical regime at each  
60 EBUS: offshore oceanic waters (OC1), non-upwelling (DW1) areas nearshore, and upwelling centers (UP1 and UP2). These  
61 points were chosen based on the consistency of the year-round upwelling centers deduced from the mean SST field and the  
62 relevance of the area as spawning and nursery emplacements for the pelagic fisheries associated with upwelling centers. Then,  
63 we compare the SST trends in the main upwelling centers of the four EBUS with those in open ocean waters through a new  
64 index,  $\alpha_{UI}$ , designed to characterize upwelling changes in the EBUS, following Bakun's (1990) hypothesis. The manuscript is  
65 organized as follows: sections 2 and 3 describe the dataset and the analysis carried out in the study. Section 4 describes the  
66 relevant results, and the results are discussed and contrasted with other studies, and finally, Section 5 summarizes and presents  
67 the conclusions.

## 68 **2. Data**

69 We based our study on the SST blended analyses for sea surface temperature of the National Ocean and Atmosphere  
70 Administration (NOAA) (Reynolds et al., 2007), which combines SST satellite retrievals with in-situ measures from ships and  
71 buoys. This dataset has a spatial resolution of  $0.25^\circ$  and covers nearly 40 years (from 1982 to 2021). Following Barton et al.  
72 (2013), the 40-years used in this study allow us to estimate significant trends. Their analysis involved a comprehensive  
73 examination of both wind stress and SST. They segmented these datasets into various subsets of different lengths. Within this  
74 analysis, the trends derived from wind datasets are not significantly different from zero for all considered subset periods.

75 In contrast, SST trends demonstrated statistical significance with a dataset of 40-years length. In addition, we incorporated  
76 reliable in-situ data in the North Pacific and the North Atlantic oceans for validation. These records were obtained from the  
77 National Buoy Data Center (NDBC) and the CalCOFI (California Cooperative Fisheries Investigations) program for the  
78 Pacific. For the Atlantic, the data were gathered from Puertos del Estado and the RaProCan (Radial Profunda de Canarias)  
79 observational program of the Spanish Institute of Oceanography in the Canary Islands (Tel et al., 2016). The in-situ data,  
80 limited to the northern hemisphere, is used to validate the satellite observations. Given the significantly larger amount of  
81 sampling density existing in the Pacific Ocean compared to the Atlantic Ocean, a lower error is expected in the reanalysis for  
82 the Pacific Ocean. We have also used the EN4 (ENhanced ocean data assimilation and climate Prediction) dataset from the  
83 Met Office Hadley Centre (Good et al., 2013), a collection of global observations from diverse sources interpolated into a  
84 monthly product and a spatial resolution of  $1^\circ$ . Due to the limited sampling in the cruise data, we cannot align it with the



85 monthly resolution of the EN4 product. To maintain statistical rigor, we choose not to employ the cruise data for the validation  
86 of EN4.

### 87 **3. Method**

#### 88 **3.1. Trends Analysis**

89 With a minimum data length (>30 years), a climate series can usually be described as a combination of multiple variabilities  
90 at different time scales. Since we are interested in the trend of the record, we removed the high-frequency variability (<1 yr)  
91 by averaging the daily NOAA SST analyses data into monthly means and removing the seasonal cycle. The seasonal cycle is  
92 a recursive signal throughout the entire record, and therefore, it does not influence the trend but induces noise in the target  
93 scale. The monthly climatology was subtracted from the record to remove the seasonal cycle. After this pre-analysis, we  
94 calculated the trend with the ordinary least square method. We evaluated the strength of these correlations using the Pearson  
95 Correlation Coefficient (PCC). The following qualitative classification will be used throughout the manuscript: Perfect (1),  
96 very high (>0.9), high (>0.7), and moderate (>0.5). Additionally, we employed the simple Mann-Kendall (MK) test to evaluate  
97 the statistical robustness (Kendall, 1975; Mann, 1945). The MK tests verify whether an n-length series holds a monotonic  
98 increase or decrease trend. In addition, we need to consider the instrumental error since, historically, a warm coastal bias is  
99 found in satellite records compared to in-situ records (Smale and Wernberg, 2009). This bias was assessed in the northern  
100 hemisphere by validating the data using in-situ observations.

101 Once the trends were calculated for all the EBUS regions, we selected areas representative of the different dynamical regimes  
102 for further analysis, to avoid mixing observations in dynamically different areas. Areas UP1 and UP2 are round-year upwelling  
103 centers, and as mentioned in Section 1, these areas are defined by relevance as nursery areas enclosed in minimum isothermal  
104 areas near the coast due to the upwelling imprint of cold water, as will be explained in detail in section 3.4. The DW1 are areas  
105 of convergence where the upwelling does not dominate on an annual average, and these areas are characterized by higher SST  
106 averages than those in the upwelling centers. The OC1 is representative of open ocean (>100km offshore) areas with trends  
107 driven by Global Warming.

#### 108 **3.2. Satellite Validation**

109 Taking advantage of the in-situ observations available in the study areas defined in Fig 2, we performed a validation through  
110 linear regression between in-situ and the deseasonalized satellite data. Records with no systematic error correspond to a linear  
111 regression slope with a value of 1 (perfect). Since the Pacific Ocean is better sampled than the Atlantic, better reanalysis  
112 performance and higher correlation are expected in the Pacific Ocean.



### 113 3.3. Angular Index of Upwelling Intensification ( $\alpha_{UI}$ )

114 To test Bakun's hypothesis, a new index, named the Angular Index of Upwelling Intensification ( $\alpha_{UI}$ ), is proposed. This new  
115 index uses the angle between the trend of the most robust upwelling cell at each EBUS and the trend at the corresponding open  
116 ocean area. If the upwelling intensifies, as Bakun proposed, the trends in the open ocean and the cell are expected to differ  
117 significantly, resulting in a higher angle between the trends. To calculate  $\alpha_{UI}$ , two vectors (in the time-temperature space) may  
118 be constructed from the upwelling ( $\overline{Up}$ ) and oceanic ( $\overline{Oc}$ ) trends. The rotation sense (clockwise or anticlockwise) is used to  
119 calculate the relative orientation of ( $\overline{Up}$ ) over ( $\overline{Oc}$ ), needing to consider an additional unitary vector normal ( $\overline{n}$ ) to both ( $\overline{Up}$ )  
120 and ( $\overline{Oc}$ ).

121 The mathematical formulation of  $\alpha_{UI}$  is

$$122 \alpha_{UI} = \text{atan2} \left( \frac{((\overline{Up} \times \overline{Oc}) \cdot \overline{n})}{\overline{Up} \cdot \overline{Oc}} \right) = \text{atan2} \left( \frac{|\overline{Up}| |\overline{Oc}| \sin(\alpha_{UI})}{|\overline{Up}| |\overline{Oc}| \cos(\alpha_{UI})} |\overline{n}| \cos(\beta) \right)$$

123 Following the right-hand rule, if the cross product of ( $\overline{Up}$ ) and ( $\overline{Oc}$ ) is anticlockwise (that is, if the open ocean trend ( $\overline{Oc}$ ) is  
124 greater than the upwelling trend ( $\overline{Up}$ )), the resulting vector of the cross product has the same orientation as  $\overline{n}$ . This implies that  
125 the dot product  $(\overline{Up} \times \overline{Oc}) \cdot \overline{n}$  is positive since the angle ( $\beta$ ) between  $\overline{n}$  and  $(\overline{Up} \times \overline{Oc})$  is  $0^\circ$ . In case the upwelling trend is  
126 greater than the open ocean trend,  $\overline{Up} \times \overline{Oc}$  results negative since  $\beta$  is now  $180^\circ$ . Note that this methodology is susceptible to  
127 the order of the vectors, as  $\overline{Up} \times \overline{Oc} = -\overline{Oc} \times \overline{Up}$ . Since we are interested in the relative position of the upwelling trend  
128 concerning the oceanic waters, the order used is  $\overline{Up} \times \overline{Oc}$ . It is important to note that the angle derived from trigonometric  
129 functions are not influence by units associated with the original vectors. Therefore, this new index is independent of  
130 temperature and time units.

131 We also performed a probabilistic assessment of uncertainties for  $\alpha_{UI}$ , considering the uncertainties associated with upwelling  
132 and open ocean SST series. For each time series, a residual error for individual data points is separately and randomly sampled  
133 10.000 times within their  $\overline{Up}$ - and  $\overline{Oc}$  uncertainties, and then used to calculate  $\alpha_{UI}$ . The standard deviation of the 10.000  
134 simulations is the uncertainty of  $\alpha_{UI}$

### 135 3.4. Selection of the upwelling centers

#### 136 Californian Upwelling System (CaIUS)

137 In the Californian system, the strongest wind stress takes place in spring in the southern portion of the CaIUS. It shifts  
138 northward in summer, with the strongest winds situated offshore of northern California around  $38^\circ$  N. This wind stress pattern  
139 diminishes as we move away from this latitude in both directions (Bakun and Nelson, 1991). Among the four regions depicted  
140 by Kämpf and Chapman (2016), the strongest upwelling occurs in two well-known upwelling centers that we have selected  
141 for the analysis in this study: Cape Mendocino (Abbott and Zion, 1987) and Point Conception (Dugdale and Wilkerson, 1989).



## 142 **Canarian Upwelling System (CanUS)**

143 Following Kämpf and Chapman (2016), the CanUS is divided into two distinct upwelling areas, which experience limited  
144 continuity of flows between them. This division arises due to the coastline interruption in the Strait of Gibraltar that leads to  
145 two upwelling areas: the Iberian Upwelling System and the Canarian Upwelling System. Given the lack of permanent  
146 upwelling centers in the Iberian Upwelling System, we have focused on the Canarian Upwelling System. Following Cropper  
147 et al. (2014), we selected the two upwelling centers (UP1 and UP2) on the cold SST cores (see Fig 2b) within the permanent  
148 upwelling area.

## 149 **Humboldt Upwelling System (HuUS)**

150 The HuUS is characterized by prominently strong upwelling zones along the Peruvian-Chilean coastline, due to the  
151 topographical influence of headlands, as described by Figueroa & Moffat, (2000) and Mesias et al., (2003). Notable regional  
152 upwelling centers encompass the continental shelf near Pisco (13.7° S), Antofagasta (21-25° S), and the Mejillones Peninsula  
153 (23° S), as well as extending further south to Coquimbo Bay (30° S), Valparaíso (33° S), and the Bay of Concepción (37° S).  
154 Moreover, in the Mejillones Peninsula (23° S), both observational (e.g., Marín, 2003) and modeling studies (Escribano et al.,  
155 2004) have revealed that the dynamics of coastal ecosystems in this area heavily rely on the generation of upwelling filaments.  
156 Additionally, the continental shelf near Pisco (13.7° S) emerges as an exceptionally productive and distinctive upwelling  
157 center. Hence, the two upwelling centers selected are the Mejillones Peninsula and Pisco.

## 158 **Benguela Upwelling System (BeUS)**

159 As Kämpf and Chapman (2016) described, within the Benguela Upwelling System, numerous upwelling centers extend along  
160 the shelf area of the Benguela Current region. These centers include Cape Frio (18.5° S), Walvis Bay (22.95° S), Lüderitz  
161 (26.45° S), Namaqualand (28.55° S), Cape Columbine (32.85° S), and Cape Town (33.95° S). Lüderitz stands out as a  
162 particularly noteworthy upwelling center within this system. As Hutchings et al. (2009) defined, it represents an intensive  
163 perennial upwelling center characterized by intense winds, high turbulence, and robust offshore transport. Another significant  
164 area of interest lies in Cape Columbine, primarily due to its biological importance (Andrews and Hutchings, 1980; Bang and  
165 Andrews, 1974; Andrews and Cram, 1969). Given these distinctive features, we have selected Lüderitz and Cape Columbine  
166 as the upwelling centers for our analysis.

## 167 **4. Results**

### 168 **4.1. Satellite Validation**

169 We first carried out a regional validation, in the northern hemisphere, with in-situ observations (Fig 2a and 2b) to test the  
170 consistency of the NOAA SST analyses between oceans. A linear fit between in-situ and satellite data gives insights into the



171 reliability of the SST data in both oceans. As described in Section 2, the in-situ dataset was divided into two categories:  
172 mooring and cruise data. Because each record has a different spatial and temporal resolution, categories are not comparable.

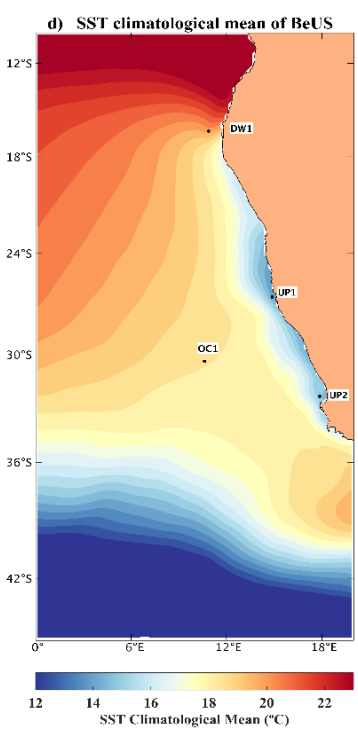
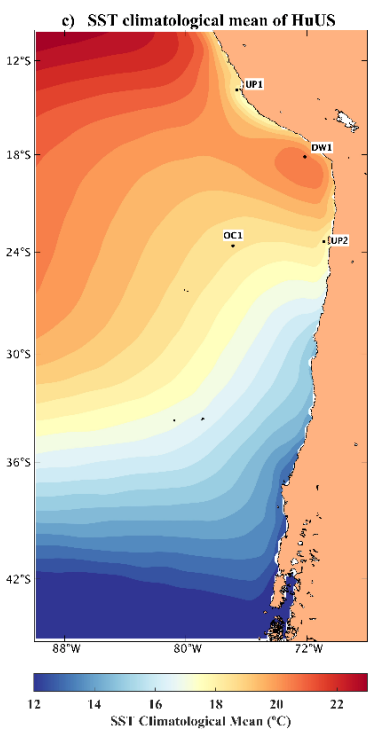
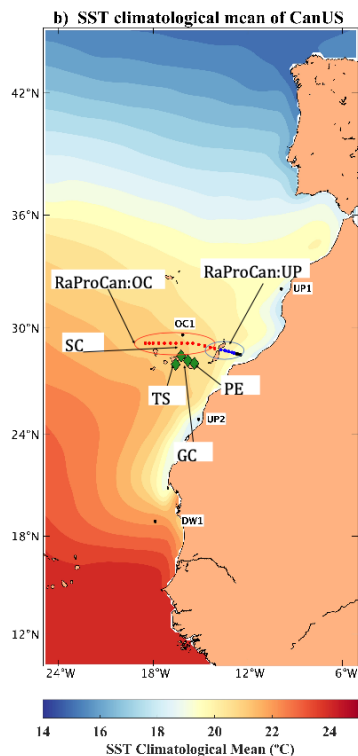
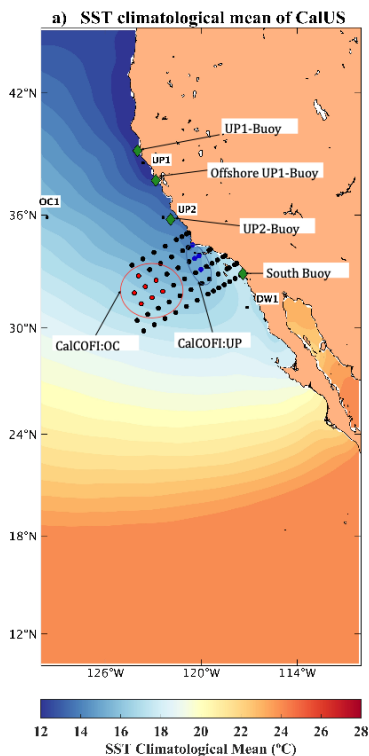




**Figure 2: Average SST maps for each of the Upwelling Systems: CalUS (a), CanUS (b), HuUS (c), and BeUS (d). Overlaid are the locations of the buoys (green diamond) and cruise data (black dots) used for the satellite validation with their corresponding names. The cruise stations were divided into upwelling and open ocean areas marked with blue and red circles, respectively. The representative points of UP, DW, and OC in each basin are shown as black dots.**

173 In the Pacific Ocean, the moorings selected were those as close as possible to the areas UP1, UP2, DW1, and OC1 described  
 174 in section 3.1 and 3.4. We found the highest correlations inside the upwelling center of this region, where the UP1-Buoy and  
 175 UP2-Buoy presented a linear regression fit of 0.99, supported by a very high correlation strength (0.94 and 0.92, respectively,  
 176 Table 1). In the area where the upwelling meets the oceanographic background, the correlation of the offshore UP1-Buoy with  
 177 the NOAA SST data decays slightly, presenting a linear slope of 0.84 and a correlation strength of 0.86. For the South-Buoy,  
 178 close to DW1, the lineal fit and correlation (0.97 and 0.92) are closer to the values inside of the upwelling cell than of the  
 179 offshore UP1-Buoy (Table 1). The results obtained for the offshore UP1-Buoy exemplify the effect of using an average large  
 180 area surrounding the upwelling centers instead of a point, as the average introduces noise by adding points where upwelling  
 181 might not be taking place, reducing the correlation in the transitional zone.

182 The cruise observations in the Pacific Ocean (CalCOFI) were divided into two different areas, open ocean (CalCOFI: OC) and  
 183 upwelling (CalCOFI: UP), and we avoid data at transitional areas, as seen in Fig 2a. The results of the linear fit between the  
 184 cruise and the reanalysis data are similar to those obtained with the mooring data (Table 1). The average within the upwelling  
 185 cell, CalCOFI: UP, has a very high linear regression value (0.91), while for the offshore stations, CalCOFI: OC, the regression  
 186 is 0.81. Nevertheless, the strength of the correlation is sensitive to the amount of data available from the cruise data in the  
 187 ocean versus the upwelling areas. Additionally, due to the time resolution of the cruise, the correlation strength is moderate  
 188 (0.68) for the CalCOFI: OC and high (0.71) for the CalCOFI: UP.

189 We also compared the EN4 dataset (Table 1, two last columns) against the NOAA SST analysis. As described in section 2,  
 190 due to the coarse temporal resolution of the cruise data, it was not possible to compare with the EN4 monthly. Overall, the  
 191 EN4 has lower correlation and regression values than the NOAA SST analyses. The correlation has the same pattern in both  
 192 datasets (NOAA and EN4): moderate in the northern locations (0.60 and 0.63) and high in the southern locations (both with  
 193 0.76), although the data length of the EN4, unlike the cruise records, is the same as the mooring.

In-situ Data	NOAA		EN4	
	Linear Slope	Correlation	Linear Slope	Correlation
UP1-Buoy (46014).	0.99	0.92	0.70	0.60
Offshore UP1-Buoy (46028).	0.84	0.86	0.72	0.63
UP2-Buoy (46225).	0.99	0.94	0.78	0.76
South-Buoy (46026).	0.97	0.92	0.77	0.76
CalCOFI: OC	0.81	0.71	-	-
CalCOFI: UP	0.91	0.68	-	-

194 **Table 1. Values of the linear regression and Pearson's correlation strength between the in-situ data (listed in the first column, with**  
 195 **the designation within the manuscript and, in brackets, the official NDBC station ID). The in-situ data are compared with the NOAA**  
 196 **SST reanalysis (second and third columns) and the EN4 product (last two columns) validation for the Pacific Ocean. The last two**  
 197 **rows are for the CALCOFI cruise data of the Pacific Ocean.**



198 In the Atlantic Ocean, the number of in-situ measurements available is more limited than in the Pacific Ocean. Therefore, the  
199 long-term records are shorter than in the Pacific Ocean and are only available in the surroundings of the Canary Islands. The  
200 results reflect these limitations since none of the linear regressions or correlation coefficients ever exceeds 0.9, unlike the  
201 results for the Pacific Ocean (Table 1). As in the Pacific Ocean, the mooring data shows a better linear regression and higher  
202 correlation coefficient than the cruise data (Table 2). The correlation coefficients for the buoys of Santa Cruz, Gran Canaria,  
203 and Tenerife Sur are high, with values of 0.89 (0.84), 0.84 (0.87), and 0.83 (0.88), respectively. The result of Las Palmas East-  
204 Buoy is comparable to the linear slope for the cruise data, 0.71. However, the Las Palmas East-Buoy has a higher correlation  
205 coefficient (0.89), which agrees with the other moorings.

206 For the cruise data, we follow the same approach as in the Pacific Ocean, dividing the data into open ocean areas (RaProCan:  
207 OC) and upwelling centers (RaProCan: UP). As occurred for the results in the Pacific, the regression is better for the upwelling  
208 cell with values of 0.73 and a correlation strength of 0.71. For the open ocean areas (RaProCan: OC), the linear slope is slightly  
209 lower (0.63) but has a higher correlation strength coefficient (0.77).

210 The EN4 dataset was also used in this areas and showed linear regressions and correlation coefficients similar to the cruise  
211 data, as shown in Table 1. In Table 2, the linear regressions of EN4 are close to the results of the moorings, even though EN4  
212 performs similarly compared to Table 1. Thus, EN4 seems a better alternative in the Atlantic Ocean than in the Pacific Ocean,  
213 but only due to the lower performance of the NOAA SST analyses in the Atlantic Ocean. However, the correlation strength of  
214 the EN4 showed lower values than NOAA SST analyses, with three out of five locations under 0.70. Hence, using the NOAA  
215 SST analyses for long-term analysis in both oceans is a better approach.

In-situ Data	NOAA		EN4	
	Linear slope	Correlation	Linear Slope	Correlation
Las Palmas East Buoy.	0.71	0.89	0.80	0.71
Santa Cruz Buoy.	0.89	0.84	0.71	0.66
Gran Canaria Buoy.	0.84	0.87	0.76	0.54
Tenerife South Buoy.	0.83	0.88	0.77	0.53
RaProCan: OC	0.63	0.77	-	-
RaProCan: UP	0.73	0.71	-	-

216 **Table 2. Values of the linear fit and correlation strength between in-situ data (listed in the first column) and both the NOAA SST**  
217 **analyses (second and third columns) and the EN4 product (last two columns) for the Atlantic Ocean. The last two rows are for the**  
218 **RaProCan cruise data of the Atlantic Ocean.**

## 219 4.2. Trend patterns on the EBUS

220 We begin by identifying the overall pattern of the long-term trends in each EBUS, which we show in Fig 3. A general pattern  
221 of cooling (negative) trends within the upwelling centers and warming (positive) trends offshore is found in most of the regions.  
222 An exception is found in the HuUS, where there is also a cooling trend offshore. This cooling mode, however, is not as  
223 pronounced as the trends onshore driven by the upwelling process. On top of these general patterns, each region presents  
224 unique features that will be described in the following paragraphs.



225 The mean trend for the CalUS (Fig 3a) is 0.10 (SD= 0.065) °C/decade. The minimum values, -0.17 °C/decade, are located near  
226 Cape Mendocino, around 43-39°N, and 32°N corresponding to the permanent upwelling centers. On the other hand, maximum  
227 values (excluding the shallower Gulf of California), reaching up to 0.20 °C/decade, are located south, at 30°N, where the winds  
228 are non-favorable for year-round upwelling, and there is convergence (Kämpf & Chapman, 2016). At around 22 °N, there is  
229 an offshore negative trend area with mean values of -0.022 °C/decade. However, the MK test revealed that these trends in the  
230 offshore area are not significant. The non-significant extensive regions in the MK test support the idea that the trends in the  
231 CalUS coastal upwelling are only statistically distinguishable from zero within the upwelling centers.

232 In the CanUS (Fig 3b), the mean trend in the region is warmer than in CalUS, with a value of 0.20 (SD= 0.047) °C/decade.  
233 The minimum values (-0.2 °C/decade) are confined to two upwelling centers in the permanent annual upwelling zones, located  
234 north of Cape Ghir and south of Cape Bojador. The maximum warming trend is 0.60°C/decade, located west of Cape Timiris  
235 in the Mauritania-Senegalese convergence zone. Because of the low spatial variability of the trend in the CanUS, the mean  
236 offshore value is the same as the average value of the entire CanUS.

237 For the HuUS (Fig 3c), the mean value of the region is 0.007 (SD= 0.099) °C/decade. a cooling signal stands out as the general  
238 pattern in the tropic, with a mean value of -0.15 °C/decade. Despite this cooling of the overall trend, there are two clear  
239 upwelling centers, at 13°N and 24°N, with minimum values of -0.36 °C/decade. In these upwelling centers, the negative trends  
240 are lower than in the open ocean at the same latitudes.

241 Finally, in the BeUS (Fig 3d), the mean trend is 0.19 (SD= 0.098) °C/decade, closer to the average of the CanUS. The two  
242 warm fronts with trends over 0.4 °C/decade can be found in both the north and south ends. In the round-year upwelling area,  
243 the Lüderitz cell, the minimum value is -0.25 °C/decade. In contrast, for the open ocean area between the two warm fronts, the  
244 values are similar to those found in the CanUS (Fig 3b), around 0.20 °C/decade.

245 The average trend for each region reveals higher open ocean warmings for the Atlantic EBUS (0.20 and 0.19 °C/decade for  
246 the CanUS and BeUS, respectively) than the Pacific Ocean (0.10 and 0.007 °C/decade, for the CalUS and HuUS, respectively),  
247 with the lower trends observed in the HuUS. However, the trends along the coast are rather heterogeneous, responding to the  
248 variability of the local upwelling dynamics, as seen in Fig 3, where several permanent upwelling centers (negative trends) exist  
249 along the coast on both continents.

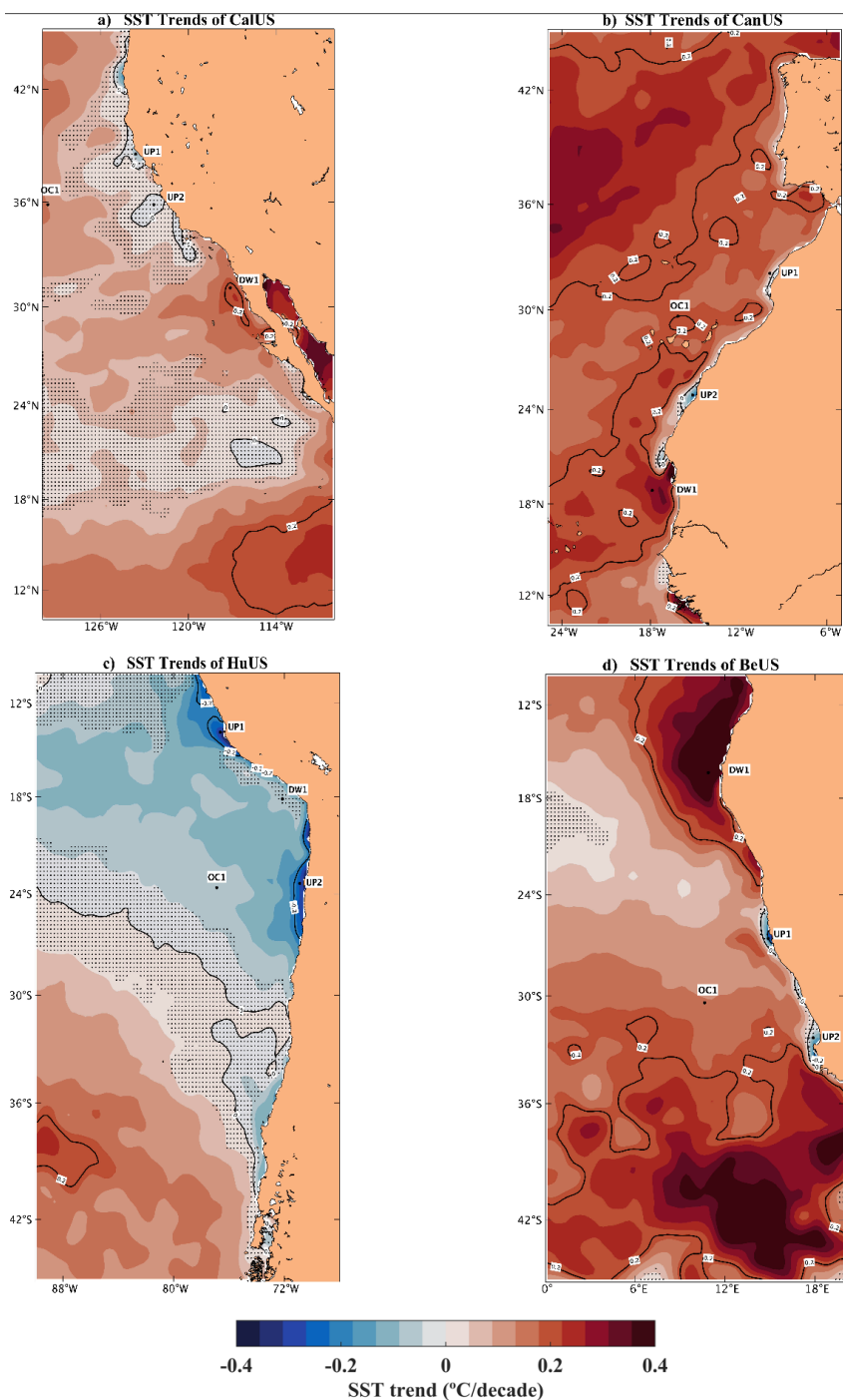


**Figure 3: Mapped SST trends (°C/decade) for the major EBUS: a) California -CalUS, b) Canary-CanUS, c) Humboldt-HuUS, and d) Benguela-BeUS. The color scale indicates the trend values at the right margin of each graph. Black-dots shaded areas indicate non-significant trends. The locations of the areas selected (UP1, UP2, OC1, and DW1) are marked with solid black circles and labeled with their names. Black contours enclosed the isotrends -0.20, 0, and 0.20°C/decade.**

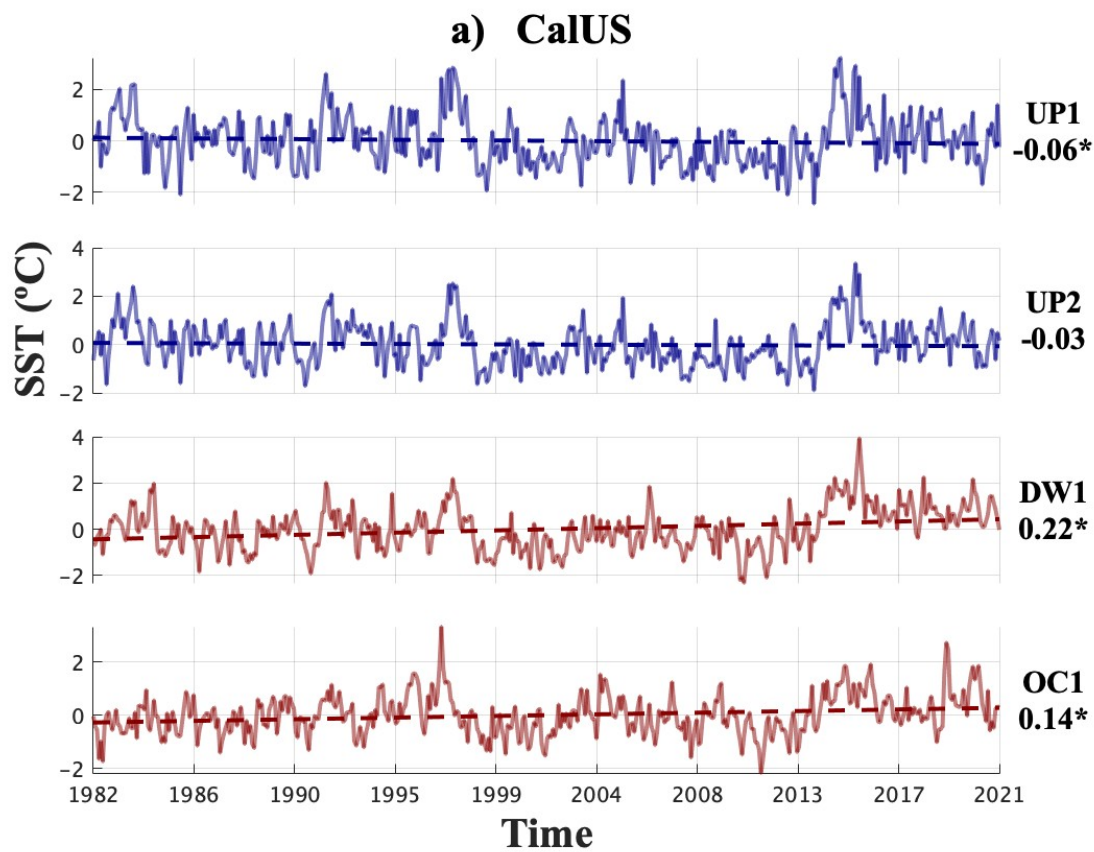


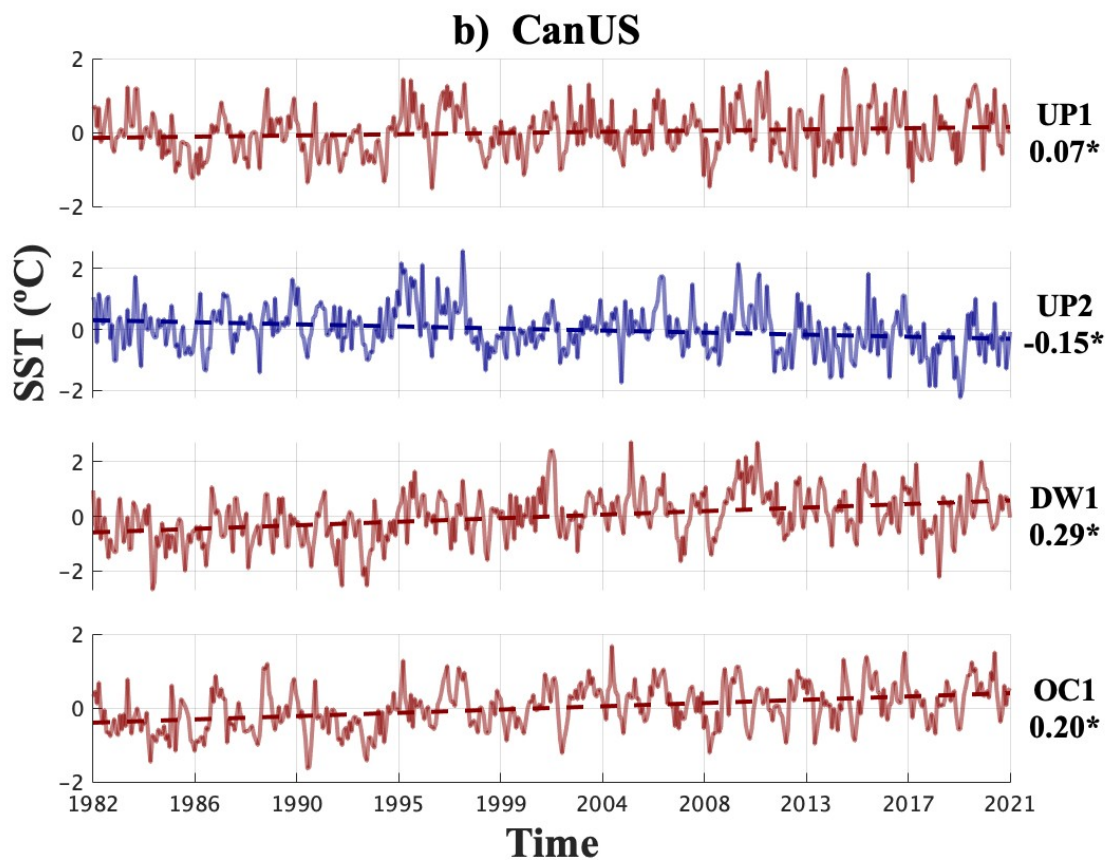
#### 250 4.3. Trends in the upwelling cells and open ocean areas.

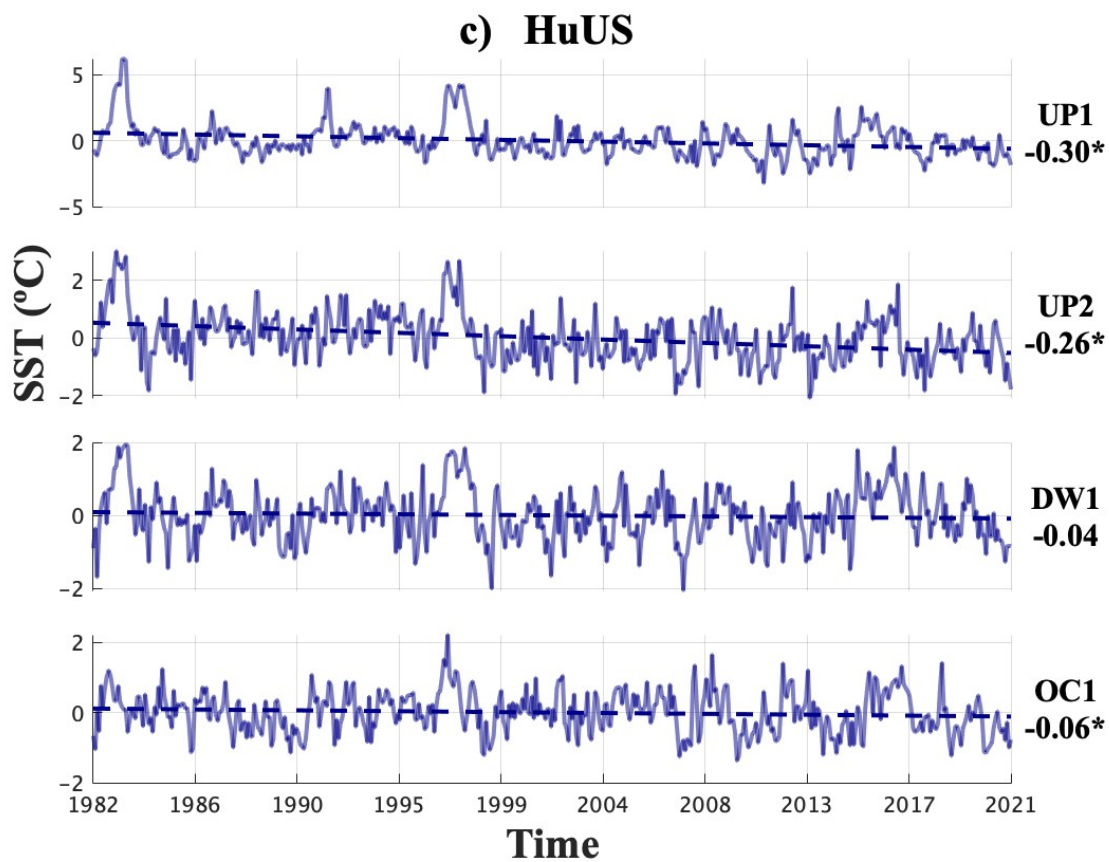
251 Although we got an overview of the long-term trends for each EBUS in the previous section, the validation of Bakun's  
252 hypothesis would require a finer resolution to describe the local dynamics of the upwelling and identify those areas where the  
253 coastal upwelling is the main forcing. In this sense, we have chosen representative points (see criteria in Section 3.4 and Figs  
254 2 and 3) of both EBUS and non-EBUS areas instead of using the large-averaged regions shown in Fig 3. These upwelling  
255 points are the upwelling centers (UP1, UP2), the nearshore areas where the upwelling is not the primary process (DW1), and  
256 the open ocean areas (OC1).

257 The CalUS presents the weakest trends of all the EBUS in both year-round upwelling centers, being  $-0.06$  °C/decade for UP1  
258 and non-significant in UP2 ( $-0.03$  °C/decade, Fig 4a). For the open ocean area, the OC1 trend is positive with a value of  $0.14$   
259 °C/decade, a lower value than the trend of  $0.22$  °C/decade of the DW1. On the Atlantic, the CanUS (Fig 4b) possesses the only  
260 positive trend ( $0.07$  °C/decade) of all the EBUS in an upwelling area (UP1). Despite UP1 being positive, the trend is closer to  
261 zero than in the OC1 ( $0.20$  °C/decade). Furthermore, the UP2 cell in the CanUS shows a trend twice as negative ( $-0.15$   
262 °C/decade) as the one on the CalUS upwelling UP1. The OC1 and DW1 areas show a warmer trend in the CanUS than in the  
263 North Pacific region (Fig 4). All of the above suggests that on the Northern Hemisphere EBUS, Bakun's hypothesis is fulfilled,  
264 and this is even more significant in the CanUS despite having been dismissed in previous studies (Sydeaman et al., 2014).  
265 In the HuUS (Fig 4c), we find a different behavior than the one seen on the other EBUS, showing negative trends in all the  
266 representative locations. The upwelling centers of the HuUS present the greatest cooling trend of all the EBUS,  $-0.30$  °C/decade  
267 at UP1 and  $-0.26$  °C/decade at UP2. As observed in CanUS, the values for HuUS in OC1 ( $0.06$  °C/decade) are similar to the  
268 ones of DW1, although DW1 is non-significant in the HuUS. Its counterpart in the Atlantic Ocean, the BeUS (Fig 3d), presents  
269 significant large negative trends in the year-round upwelling areas ( $-0.23$  °C/decade for UP1 and  $-0.10$  °C/decade for the UP2)  
270 and positive trends in OC1,  $0.14$  °C/decade. The trend of the DW1 is the warmest ( $0.57$  °C/decade) found in all the EBUS, and  
271 it is related to the warm inflow from the Indian Ocean.

272 Overall, the trends show warming in the OC1 areas while cooling in the upwelling areas, except for the HuUS, where the trend  
273 at the OC1 is also slightly negative. The contrast between the trends of upwelling and open ocean areas found throughout the  
274 EBUS indicates upwelling intensification. To quantify this intensification, it is necessary to have an index that compares the  
275 intensification of the upwelling with the global warming trend on the open ocean area, that can be compared for all the EBUS.  
276 To compare the intensification between upwellings and to further understand the impact of the oceanic background on these  
277 trends, we will use the index  $\alpha_{UI}$  described before to normalize the trends of each EBUS.







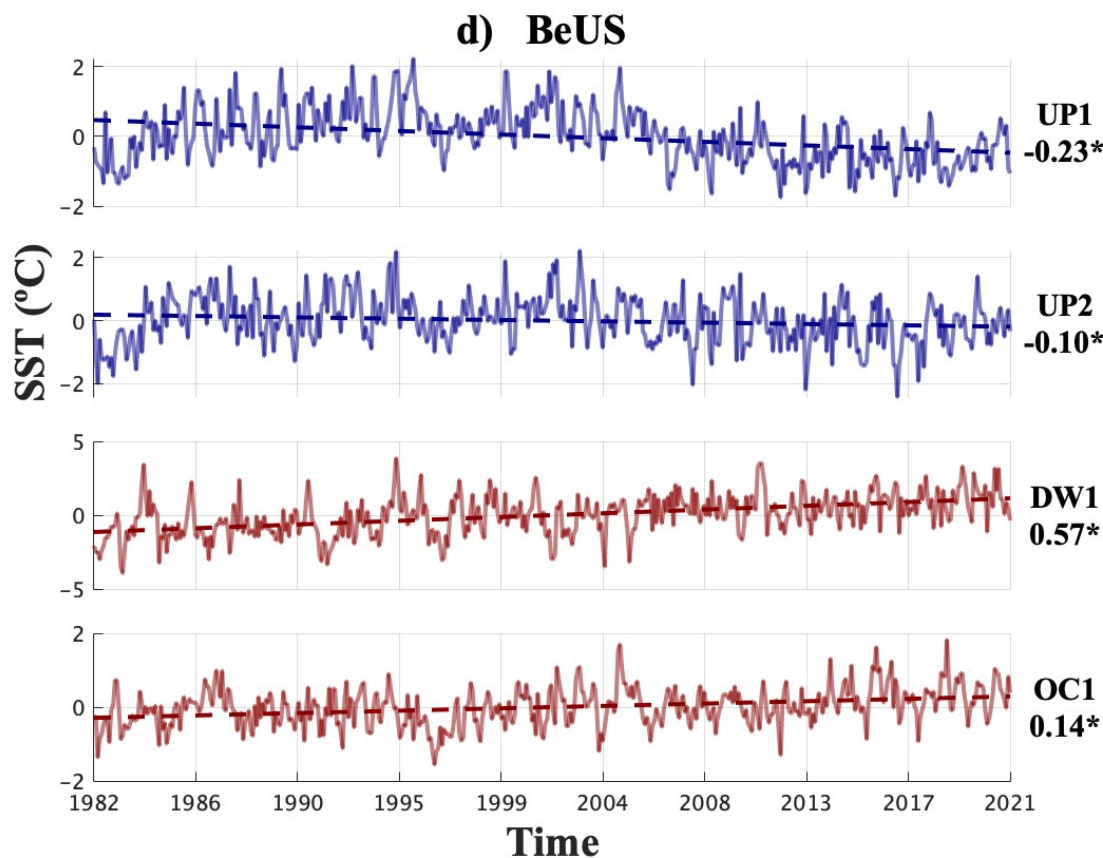


**Figure 4:** SST time series and trends ( $^{\circ}\text{C}/\text{decade}$ ) for the selected areas for each one of the EBUS (DW1, UP1, and UP2) and the areas representative of the open ocean (OC1) in each EBUS: a) California, b) Canary, c) Humboldt and d) Benguela. The blue lines are for negative (cooling) trends, and the red ones are for positive (warming) trends. On the right side of the Y-axis, the trends are shown in  $^{\circ}\text{C}/\text{decade}$ , along with the area's label and significance. Significant trends ( $p\text{-value}<0.05$ ) are marked with the symbol "\*" next to their value.

278 **4.4. The relation between Oceanic and EBUS trends.**

279 Global warming induces the increase of oceanic SST, and under Bakun's hypothesis, it also enhances the favorable upwelling  
280 winds responsible for intensifying the upwelling areas. We define an angle between the upwelling and oceanic trends, as  
281 described in the methodology section, to discern Bakun's hypothesis from the global increase in SST. As described previously  
282 (Fig 4), the upwelling centers UP1 (except for the CanUS, where UP2 will be used due to the warming detected on UP1 in  
283 Section 4.3) have the strongest cooling, and we will use these trends (hereafter, in this section UP) to create the angle contrasts  
284 with the positive warming trend of the open ocean (OC1) area for each EBUS (Fig 4).

285 For CanUS, the  $\alpha_{UI}$  obtained between the UP and OC1 trends is  $20^{\circ}\pm 2^{\circ}$  whereas it is  $11^{\circ}\pm 3^{\circ}$  in the CalUS,  $21^{\circ}\pm 2^{\circ}$  for the  
286 BeUS, and  $14^{\circ}\pm 3^{\circ}$  for the HuUS. The smallest angle is found in the CalUS because of the low cooling and warming trends  
287 described in Section 4.3. This result for the CalUS is coherent with the overall non-significant trends in the Mann-Kendall test



288 (Fig 3a). The BeUS and CanUS have the highest contrast between the two regression lines (recall that we observed similar UP  
289 and OC1 trends in the Atlantic Ocean in Section 4.3) presenting similar  $\alpha_{UI}$ .  
290 The BeUS and CanUS show a weaker negative trend than the HuUS, but the oceanic background at the HuUS leads to a  
291 smaller angle. At the HuUS, a negative SST trend is observed for the whole study area. The hypotheses existing suggest that  
292 this trend is led either by a stronger La Niña (Meehl et al., 2016) or related to the Southern Ocean SST changes (Kang et al.,  
293 2023b, a). Nevertheless, at the HuUS, we have the most prominent upwelling negative trend. However, when normalized with  
294 the open ocean trend, the Bakun's effect is reduced. In the annual upwelling series of CalUS and HuUS, there are two prominent  
295 spikes associated with El Niño appeared around 1983 and 1997.  
296 In general, we found positive  $\alpha_{UI}$  for all the EBUS, supporting the intensification of the upwelling-oceanic gradient, as expected  
297 from Bakun's hypothesis.

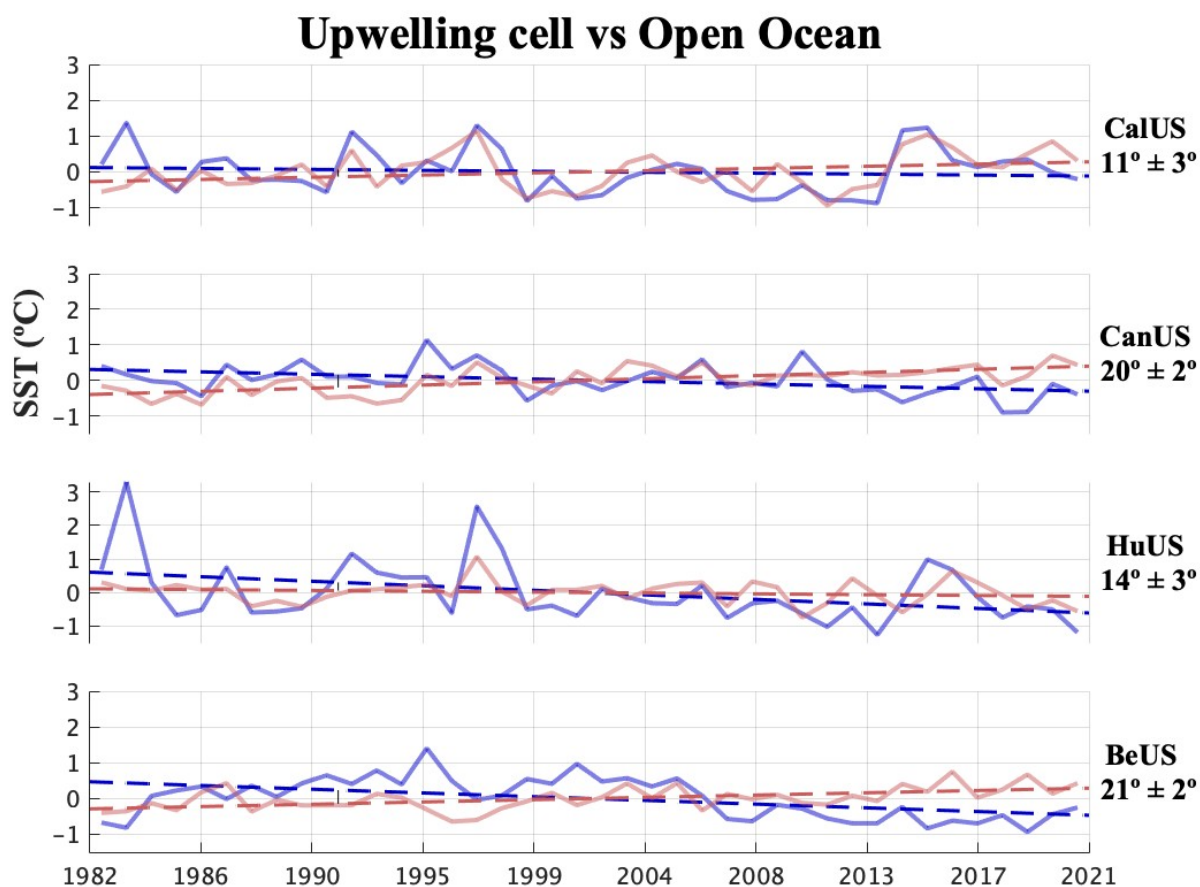


**Fig. 5. EBUS SST trends (°C/decade) against non-EBUS areas trends for each region. The EBUS annual series (continuous line) and trend (dotted line) are shown in blue; the same is true for the non-EBUS but is represented in red. On the opposite side of the Y-axis is labeled the  $\alpha_{UI}$  with their corresponding EBUS.**



## 298 **5 Discussion and Conclusions.**

299 The future of the EBUS under global warming conditions remains uncertain. The controversies around Bakun's hypothesis -  
300 an intensification of the upwelling due to the increase of the continental low-pressure system driven by global warming- have  
301 its source in (1) discrepancies between wind stress datasets and (2) differences in the methodologies used.

302 On one hand, Barton et al. (2013) highlighted a lack of consensus among various wind datasets, since they did not observe  
303 statistically significant changes in the meridional (upwelling-favorable) wind. These discrepancies in wind data are consistent  
304 with those noted by Narayan et al. (2010), who, despite finding significantly increasing in coastal upwelling areas when using  
305 COADS wind stress, also found that the NCEP/NCAR wind stress indicated a significant decrease in the upwelling off NW  
306 Africa, and a non-statistically significant trend for Lüderitz, California, and the Peruvian upwelling areas. Furthermore, they  
307 also observed that the ERA-40 dataset showed an increasing coastal upwelling in the NW African and Peruvian upwelling  
308 areas but a decreasing in the California upwelling areas, with a non-statistically significant trend in the Lüderitz upwelling  
309 areas. Therefore, using wind data as a proxy for upwelling leads to a wide spread of results as it strongly depends on the data  
310 product used.

311 On the other hand, SST-based indexes are usually constructed from thermal differences between coastal and offshore SST  
312 areas taken at the same latitude and following the coastline (Benazzouz et al., 2014; Santos et al., 2012; Gómez-Gesteira et al.,  
313 2008). This methodology does not consider the regional upwelling dynamics, and average upwelling centers with areas without  
314 upwelling. Abrahams et al. (2021) introduced an upwelling metric based on marine heatwave detection techniques, examining  
315 favorable upwelling winds and SST data together. Their findings revealed a strong association between a decrease in SST and  
316 an increase in upwelling intensity. Their novel methodology holds significant importance in unraveling the connection between  
317 the physical upwelling phenomenon and its ecological impacts. Furthermore, they successfully establish a link between  
318 decreased SST and changes in upwelling intensity, even when trends in wind dynamics do not fully account for the upwelling  
319 response, reinforcing the notion that SST is a suitable proxy for upwelling intensity. However, their SST metrics exhibited  
320 inconsistencies across upwelling areas, except for the Humboldt system. These inconsistencies may be due to the averaging of  
321 data across extensive areas, mixing upwelling areas with areas without the associated cold water of upwelling. Abrahams et  
322 al. (2021) also explored these metrics in upwelling-favorable winds data, and their results indicated that decadal trends were  
323 generally not significant. As previously discussed, wind products often yield contradictory results despite their direct relevance  
324 to upwelling. Hence, our study complements Abrahams et al. (2021) since we have focused on SST to understand longer terms  
325 changes in the upwelling intensity, using areas with optimal signal-to-noise ratio, namely the upwelling centers, revealing  
326 upwelling-related cool water in all Eastern Boundary Upwelling Systems (EBUS).

327 Therefore, in this study, we assess Bakun's hypothesis from a regional perspective, by using SST trends at locations  
328 representative of upwelling and of an open oceanic reference location for each different EBUS. Furthermore, to assess the  
329 strength of the net upwelling intensification, we proposed an index that allows inter-basin comparisons attending to their  
330 regional background. SST, often used as an indicator of coastal upwelling, can be influenced by various factors, such as



331 changes in surface mixing and offshore storm activity. However, in our long-term analysis of monthly and deseasonalized SST  
332 records, the seasonal and synoptic processes have minimal influence on the SST-upwelling intensity relationship. Moreover,  
333 Wang et al. (2015) explored the connection between sea-land thermal gradients and offshore Ekman transport using the CMIP5  
334 models. Their findings underscore the significant link between thermal gradients and offshore Ekman transport, even under  
335 greenhouse gas emission scenarios. McGregor et al. (2007) and Santos et al. (2012) also support this relationship, emphasizing  
336 significant correlations between coastal SST and offshore Ekman transport, reinforcing the utility of coastal SST as a proxy  
337 for assessing upwelling intensity.

338 To assess the quality of our results, we validated the NOAA SST reanalysis with in-situ data from both the Atlantic and Pacific  
339 Oceans before estimating the trends in all EBUS. Overall, the Atlantic Ocean had lower correlations with the satellite data than  
340 the Pacific Ocean, likely due to shorter in-situ records. Nevertheless, we found high and robust correlation coefficients ( $>0.7$ )  
341 that sustain the satellite SST trends in oceanic and upwelling areas. We observed negative SST trends in all the EBUS, being  
342 stronger in the southern hemisphere (the strongest located in the HuUS-UP1 showing a  $-0.30^{\circ}\text{C}/\text{decade}$ ) than in the northern  
343 hemisphere (the weakest in the CalUS-UP2 with a trend of  $-0.06^{\circ}\text{C}/\text{decade}$ ). Our results are consistent with the meta-analysis  
344 by Sydeman et al. (2014), who concluded that a significant intensification of upwelling exists from observational and model  
345 data, except for the case of CanUS.

346 Other studies have investigated the SST trends in the EBUS but with an approach that did not consider the heterogeneity of  
347 the upwelling areas. For instance, in the CalUS, Seabra et al. (2019) reported a  $0.06^{\circ}\text{C}/\text{decade}$  warming rate. However, their  
348 approach involved averaging a 500 km nearshore area, excluding non-significant regions. Thus, almost half of the extension  
349 was not considered, resulting in the average of different dynamical areas and the exclusion of upwelling centers. Belkin et al.  
350 (2009) performed a similar analysis but included the entire CalUS nearshore area. They found a net change of  $-0.035^{\circ}\text{C}/\text{decade}$   
351 over the 1982-2007 period, agreeing in sign with our study but showing a higher (more positive) rate due to the use of a large  
352 average. In contrast, Siemer et al. (2021) found negative trends of  $-0.14^{\circ}\text{C}/\text{decade}$  for the CanUS permanent upwelling area,  
353 like our results ( $-0.15^{\circ}\text{C}/\text{decade}$ ). However, this trend fades away and becomes positive when they average the whole coastal  
354 upwelling area, highlighting the relevance of the methodology used in this study. Likewise, many studies carried out in this  
355 area present positive trends for the upwelling due to the method used (Demarcq, 2009; Belkin, 2009; Seabra et al., 2019). In  
356 line with our study, Seabra et al. (2019) found the coolest trends ( $-0.07 \pm 0.08^{\circ}\text{C}/\text{decade}$ ) in the HuUS. However, like in other  
357 EBUS, using average areas increased the trend values. This pattern is also observed by Belkin et al. (2009), where the net  
358 change of the average nearshore area results in  $-0.05^{\circ}\text{C}/\text{decade}$ . For the BeUS, similar to CanUS, averaging the entire coastal  
359 upwelling area results in the fading of the observed upwelling trend. Hence, a warming rate of  $0.17^{\circ}\text{C}/\text{decade}$  is found in  
360 Seabra et al. (2019). In contrast, Santos et al. (2012) investigated trends close to the shore without averaging areas and found  
361 a negative trend of the BeUS, strongly agreeing with our results ( $-0.13^{\circ}\text{C}/\text{decade}$ ).

362 While all the upwelling trends are negative and support the Bakun's hypothesis, the oceanic trends behave differently across  
363 basins. We observed warming in all the open ocean areas except in the HuUS, where a cooling of  $-0.06^{\circ}\text{C}/\text{decade}$  is observed.



364 Dong & Zhou (2014) studied the influence of the IPO on Global Warming trends. Their EOF analysis results indicate that the  
365 transition to the negative phase of the IPO modes is responsible for the cooling trends observed in the Pacific.  
366 The warming in the CalUS and BeUS is  $0.14^{\circ}\text{C}/\text{decade}$ , while this trend is slightly more prominent in the CanUS. Seabra et  
367 al. (2019) revealed oceanic warming rates ( $0.06^{\circ}\text{C}/\text{decade}$ ) on the averaged upwelling in CalUS lower than the OC1 trend  
368 ( $0.14^{\circ}\text{C}/\text{decade}$ ). The open ocean positive trend of the CanUS is identical to the one in Siemer et al. (2021) and further agrees  
369 with other studies (Good et al., 2007; Signorini et al., 2015; Belkin, 2009). The result of Seabra et al. (2019) in HuUS also  
370 showed a very similar trend ( $-0.07^{\circ}\text{C}$ ) compared with our OC1 trend. Finally, in the BeUS, a good agreement is found with  
371 the average warming rate of Seabra et al. (2019). Our study demonstrates good agreement with existing literature on oceanic  
372 trends despite the differences in methodologies employed.

373 Although long-term changes, such as the North Atlantic Oscillation or the Pacific Oscillation, can impact the SST gradient,  
374 their effect would not surpass the ability of our analysis to support Bakun's hypothesis. In that sense, Nayaran et al. (2010)  
375 found that correlations between upwelling indices and climate indices like the Atlantic Multidecadal Oscillation Index (AMOI)  
376 lack significance. Similarly, the North Atlantic Oscillation Index (NAOI) exhibits a notable negative correlation with  
377 meridional wind stress off NW Africa, yet its correlation with the SST index remains insignificant. In the case of the CalUS,  
378 the Pacific Decadal Oscillation Index (PDOI) shows a weak but statistically significant correlation with the coastal upwelling  
379 SST index off California. However, no substantial correlation is found with alongshore wind stress. Cross-correlation analyses  
380 also reveal a lack of significant correlations across various time lags. These results suggest that long-term climate indices may  
381 not strongly influence coastal upwelling dynamics.

382 To assess Bakun's hypothesis and, thus, the upwelling capacity to overcome the oceanic warming effect, we define the angle  
383 ( $\alpha_{UI}$ , readers are referred to section 3.3) between oceanic water and upwelling trends. Because this new index is directly based  
384 on trends, it captures only the low-frequency variability. Additionally, we verified the method's robustness using a probabilistic  
385 assessment of the uncertainties that showed consistent intensifications for all EBUS (Fig 5). This new approach differs from  
386 the traditional trend analysis since it normalizes the upwelling trends by comparing them with open ocean changes.

387 The EBUS in the Pacific Ocean yields minimum  $\alpha_{UI}$  ( $10^{\circ}\pm 3^{\circ}$  and  $14^{\circ}\pm 3^{\circ}$  for CICME and HuUS, respectively), which is  
388 consistent with the low signal-to-noise ratio of global warming on this ocean, given its natural variability. The overall cooling  
389 signal caused by the IPO enhances the HuUS open ocean negative trends. Still, our index normalizes the upwelling trend to  
390 the full basin variability, suggesting the possibility of a mild Bakun effect even at the HuUS. In the Atlantic Ocean, the  $\alpha_{UI}$  for  
391 the CanUS and BeUS are  $20^{\circ}\pm 2^{\circ}$  and  $21^{\circ}\pm 2^{\circ}$ , respectively, twice as large as on the Pacific Ocean. The  $\alpha_{UI}$  presents wider angles  
392 at the southern hemisphere EBUS than in the northern hemisphere EBUS. Nevertheless, our results show a significant  
393 difference between oceanic and coastal trends reflected in positive  $\alpha_{UI}$  in all EBUS (Fig 5).

394 In summary, in this study, we use SST at discrete locations to explore the Bakun's hypothesis in the four major EBUS. Cooling  
395 trends are observed for all upwelling areas (the strongest in the HuUS and the weakest in the CalUS), and mainly warming  
396 trends offshore except for the HuUS. In addition, a novel index  $\alpha_{UI}$  that normalizes the upwelling trends to their background  
397 open ocean trend is proposed. This index is easy to estimate, allows interbasin trend comparisons, and helps understand the



398 role of changing upwellings in a changing climate. The index reveals that the Bakun hypothesis is fulfilled in all four EBUS,  
399 although the Atlantic Basin shows a higher intensification effect than the Pacific Ocean, and slightly stronger in the southern  
400 hemisphere than in the northern hemisphere.

#### 401 **Data availability.**

402 The moored data analyzed in this study are available at <https://www.ndbc.noaa.gov/> and [https://www.puertos.es/es-](https://www.puertos.es/es-es/oceanografia/Paginas/portus.aspx)  
403 [es/oceanografia/Paginas/portus.aspx](https://www.puertos.es/es-es/oceanografia/Paginas/portus.aspx) for the Pacific and Atlantic Ocean, respectively. The cruise data are also available  
404 at <https://calcofi.org/data/> for the Pacific Ocean and upon request from the author in the case of the Atlantic Ocean. And for  
405 the Satellite-based SST data, the NOAA reanalysis product are available from [https://www.ncei.noaa.gov/data/sea-surface-](https://www.ncei.noaa.gov/data/sea-surface-temperature-optimum-interpolation/access/avhrr-only/)  
406 [temperature-optimum-interpolation/access/avhrr-only/](https://www.ncei.noaa.gov/data/sea-surface-temperature-optimum-interpolation/access/avhrr-only/).

#### 407 **Author contribution**

408 M, Gutierrez-Guerra processed the data, and carried out all data analyses. M, Gutierrez-Guerra wrote the original paper with  
409 contributions from M, Gutierrez-Guerra, M.D, Perez-Hernandez and P, Velez. M.D, Perez-Hernandez and P, Velez supervised  
410 the study. All authors reviewed and edited the final paper.

#### 411 **Competing interests**

412 The contact author has declared that none of the authors has any competing interest.

#### 413 **Acknowledges**

414 This article is a publication of the Unidad Océano y Clima from Universidad de Las Palmas de Gran Canaria, an R&D&I  
415 CSIC-associate unit. This work has been completed as part of the doctoral program in Oceanography and Global Change at  
416 the Instituto de Oceanografía y Cambio Global (IOCAG). M.A. Gutiérrez-Guerra acknowledges the INVESTIGO grant  
417 program of “Plan de Recuperación, Transformación y Resiliencia – Next Generation EU”.

#### 418 **References**

419 Abbott, M. R. and Zion, P. M.: Spatial and temporal variability of phytoplankton pigment off northern California during  
420 Coastal Ocean Dynamics Experiment 1, *J Geophys Res Oceans*, 92, 1745–1755, <https://doi.org/10.1029/JC092IC02P01745>,  
421 1987.



- 422 Abrahams, A., Schlegel, R. W., and Smit, A. J.: Variation and Change of Upwelling Dynamics Detected in the World's Eastern  
423 Boundary Upwelling Systems, *Front Mar Sci*, 8, 626411, <https://doi.org/10.3389/FMARS.2021.626411/BIBTEX>, 2021.
- 424 Andrews, W. R. H. and Cram, D. L.: Combined Aerial and Shipboard Upwelling Study in the Benguela Current, *Nature* 1969  
425 224:5222, 224, 902–904, <https://doi.org/10.1038/224902a0>, 1969.
- 426 Andrews, W. R. H. and Hutchings, L.: Upwelling in the Southern Benguela Current, *Prog Oceanogr*, 9, 1–81,  
427 [https://doi.org/10.1016/0079-6611\(80\)90015-4](https://doi.org/10.1016/0079-6611(80)90015-4), 1980.
- 428 Bakun, A.: Global climate change and intensification of coastal ocean upwelling, *Science* (1979), 247, 198–201,  
429 <https://doi.org/10.1126/science.247.4939.198>, 1990.
- 430 Bakun, A. and Nelson, C. S.: The Seasonal Cycle of Wind-Stress Curl in Subtropical Eastern Boundary Current Regions, *J*  
431 *Phys Oceanogr*, 21, 1815–1834, [https://doi.org/https://doi.org/10.1175/1520-0485\(1991\)021<1815:TSCOWS>2.0.CO;2](https://doi.org/https://doi.org/10.1175/1520-0485(1991)021<1815:TSCOWS>2.0.CO;2),  
432 1991.
- 433 Bang, N. and Andrews, W.: Direct current measurements of a shelf-edge frontal jet in the southern Benguela system, *J Mar*  
434 *Res*, 32, 1974.
- 435 Barton, E. D., Field, D. B., and Roy, C.: Canary current upwelling: More or less?, *Prog Oceanogr*, 116, 167–178,  
436 <https://doi.org/10.1016/j.pocean.2013.07.007>, 2013.
- 437 Belkin, I. M.: Rapid warming of Large Marine Ecosystems, *Prog Oceanogr*, 81, 207–213,  
438 <https://doi.org/10.1016/j.pocean.2009.04.011>, 2009.
- 439 Benazzouz, A., Mordane, S., Orbi, A., Chagdali, M., Hilmi, K., Atillah, A., Lluís Pelegrí, J., and Hervé, D.: An improved  
440 coastal upwelling index from sea surface temperature using satellite-based approach – The case of the Canary Current  
441 upwelling system, *Cont Shelf Res*, 81, 38–54, <https://doi.org/10.1016/j.csr.2014.03.012>, 2014.
- 442 Cropper, T. E., Hanna, E., and Bigg, G. R.: Spatial and temporal seasonal trends in coastal upwelling off Northwest Africa,  
443 1981–2012, *Deep Sea Research Part I: Oceanographic Research Papers*, 86, 94–111,  
444 <https://doi.org/10.1016/J.DSR.2014.01.007>, 2014.
- 445 Demarcq, H.: Trends in primary production, sea surface temperature and wind in upwelling systems (1998-2007), *Prog*  
446 *Oceanogr*, 83, 376–385, <https://doi.org/10.1016/j.pocean.2009.07.022>, 2009.
- 447 Dugdale, R. C. and Wilkerson, F. P.: New production in the upwelling center at Point Conception, California: temporal and  
448 spatial patterns, *Deep Sea Research Part A. Oceanographic Research Papers*, 36, 985–1007, <https://doi.org/10.1016/0198->  
449 [0149\(89\)90074-5](https://doi.org/10.1016/0198-0149(89)90074-5), 1989.
- 450 Ekman, V. W.: On the Influence of the Earth's Rotation on Ocean-Currents, *Almqvist & Wiksells, Uppsala [Sweden]*, 1–52  
451 pp., 1905.
- 452 Escribano, R., Daneri, G., Farías, L., Gallardo, V. A., González, H. E., Gutiérrez, D., Lange, C. B., Morales, C. E., Pizarro,  
453 O., Ulloa, O., and Braun, M.: Biological and chemical consequences of the 1997–1998 El Niño in the Chilean coastal upwelling  
454 system: a synthesis, *Deep Sea Research Part II: Topical Studies in Oceanography*, 51, 2389–2411,  
455 <https://doi.org/10.1016/J.DSR2.2004.08.011>, 2004.



- 456 Figueroa, D. and Moffat, C.: On the influence of topography in the induction of coastal upwelling along the Chilean Coast,  
457 *Geophys Res Lett*, 27, 3905–3908, <https://doi.org/10.1029/1999GL011302>, 2000.
- 458 García-Reyes, M., Sydeman, W. J., Schoeman, D. S., Rykaczewski, R. R., Black, B. A., Smit, A. J., and Bograd, S. J.: Under  
459 pressure: Climate change, upwelling, and eastern boundary upwelling ecosystems, *Front Mar Sci*, 2, 1–10,  
460 <https://doi.org/10.3389/fmars.2015.00109>, 2015.
- 461 Gómez-Gesteira, M., De Castro, M., Álvarez, I., Lorenzo, M. N., Gesteira, J. L. G., and Crespo, A. J. C.: Spatio-temporal  
462 upwelling trends along the Canary upwelling system (1967-2006), *Ann N Y Acad Sci*, 1146, 320–337,  
463 <https://doi.org/10.1196/annals.1446.004>, 2008.
- 464 Good, S. A., Corlett, G. K., Remedios, J. J., Noyes, E. J., and Llewellyn-Jones, D. T.: The global trend in sea surface  
465 temperature from 20 years of advanced very high resolution radiometer data, *J Clim*, 20, 1255–1264,  
466 <https://doi.org/10.1175/JCLI4049.1>, 2007.
- 467 Good, S. A., Martin, M. J., and Rayner, N. A.: EN4: Quality controlled ocean temperature and salinity profiles and monthly  
468 objective analyses with uncertainty estimates, *J Geophys Res Oceans*, 118, 6704–6716,  
469 <https://doi.org/10.1002/2013JC009067>, 2013.
- 470 Hutchings, L., van der Lingen, C. D., Shannon, L. J., Crawford, R. J. M., Verheye, H. M. S., Bartholomae, C. H., van der Plas,  
471 A. K., Louw, D., Kreiner, A., Ostrowski, M., Fidel, Q., Barlow, R. G., Lamont, T., Coetzee, J., Shillington, F., Veitch, J.,  
472 Currie, J. C., and Monteiro, P. M. S.: The Benguela Current: An ecosystem of four components, *Prog Oceanogr*, 83, 15–32,  
473 <https://doi.org/10.1016/j.pocean.2009.07.046>, 2009.
- 474 Kämpf, J. and Chapman, P.: *Upwelling Systems of the World*, <https://doi.org/10.1007/978-3-319-42524-5>, 2016.
- 475 Kang, S. M., Yu, Y., Deser, C., Zhang, X., Kang, I. S., Lee, S. S., Rodgers, K. B., and Ceppi, P.: Global impacts of recent  
476 Southern Ocean cooling, *Proc Natl Acad Sci U S A*, 120, e2300881120,  
477 [https://doi.org/10.1073/PNAS.2300881120/SUPPL\\_FILE/PNAS.2300881120.SAPP.PDF](https://doi.org/10.1073/PNAS.2300881120/SUPPL_FILE/PNAS.2300881120.SAPP.PDF), 2023a.
- 478 Kang, S. M., Ceppi, P., Yu, Y., and Kang, I. S.: Recent global climate feedback controlled by Southern Ocean cooling, *Nature*  
479 *Geoscience* 2023 16:9, 16, 775–780, <https://doi.org/10.1038/s41561-023-01256-6>, 2023b.
- 480 Kendall, M.: *Rank correlation methods* (4th edn.) Charles Griffin, San Francisco, CA, 8, 875, 1975.
- 481 Mann, H. B.: *Nonparametric Tests Against Trend*, *Econometrica*, 13, 245, <https://doi.org/10.2307/1907187>, 1945.
- 482 Marín, C.: Upwelling shadows at Mejillones Bay (northern Chilean coast): a remote sensing in situ analysis, *Investigaciones*  
483 *Marinas*, 31, 47–55, 2003.
- 484 McGregor, H. V., Dima, M., Fischer, H. W., and Mülitza, S.: Rapid 20th-century increase in coastal upwelling off northwest  
485 Africa, *Science* (1979), 315, 637–639, <https://doi.org/10.1126/science.1134839>, 2007.
- 486 Meehl, G. A., Hu, A., Santer, B. D., and Xie, S. P.: Contribution of the Interdecadal Pacific Oscillation to twentieth-century  
487 global surface temperature trends, *Nature Climate Change* 2016 6:11, 6, 1005–1008, <https://doi.org/10.1038/nclimate3107>,  
488 2016.



- 489 Mesias, J. M., Matano, R. P., and Strub, P. T.: Dynamical analysis of the upwelling circulation off central Chile, *J Geophys*  
490 *Res Oceans*, 108, 3085, <https://doi.org/10.1029/2001JC001135>, 2003.
- 491 Narayan, N., Paul, A., Mulitza, S., and Schulz, M.: Trends in coastal upwelling intensity during the late 20th century, *Ocean*  
492 *Science*, 6, 815–823, <https://doi.org/10.5194/OS-6-815-2010>, 2010.
- 493 Pauly, D. and Christensen, V.: Primary production required to sustain global fisheries, *Nature*, 376, 279–279,  
494 <https://doi.org/10.1038/376279b0>, 1995.
- 495 Reynolds, R. W., Smith, T. M., Liu, C., Chelton, D. B., Casey, K. S., and Schlax, M. G.: Daily high-resolution-blended analyses  
496 for sea surface temperature, *J Clim*, 20, 5473–5496, <https://doi.org/10.1175/2007JCLI1824.1>, 2007.
- 497 Rykaczewski, R. R., Dunne, J. P., Sydeman, W. J., García-Reyes, M., Black, B. A., and Bograd, S. J.: Poleward displacement  
498 of coastal upwelling-favorable winds in the ocean’s eastern boundary currents through the 21st century, *Geophys Res Lett*, 42,  
499 6424–6431, <https://doi.org/10.1002/2015GL064694>, 2015.
- 500 Sambe, B., Tandstad, M., Caramelo, A. M., and Brownd, B. E.: Variations in productivity of the Canary Current Large Marine  
501 Ecosystem and their effects on small pelagic fish stocks, *Environ Dev*, 17, 105–117,  
502 <https://doi.org/10.1016/j.envdev.2015.11.012>, 2016.
- 503 Santos, F., deCastro, M., Gómez-Gesteira, M., and Álvarez, I.: Differences in coastal and oceanic SST warming rates along  
504 the Canary upwelling ecosystem from 1982 to 2010, *Cont Shelf Res*, 47, 1–6, <https://doi.org/10.1016/j.csr.2012.07.023>, 2012.
- 505 Seabra, R., Varela, R., Santos, A. M., Gómez-Gesteira, M., Meneghesso, C., Wethey, D. S., and Lima, F. P.: Reduced nearshore  
506 warming associated with eastern boundary upwelling systems, *Front Mar Sci*, 6, 445128,  
507 <https://doi.org/10.3389/FMARS.2019.00104/BIBTEX>, 2019.
- 508 Sherman, K. and Hempel, G.: The UNEP Large Marine Ecosystem Report: A perspective on changing conditions in LMEs of  
509 the world’s Regional Seas, *UNEP Regional Seas Reports and Studies*, 2008.
- 510 Siemer, J. P., Machín, F., González-Vega, A., Arrieta, J. M., Gutiérrez-Guerra, M. A., Pérez-Hernández, M. D., Vélez-Belchí,  
511 P., Hernández-Guerra, A., and Fraile-Nuez, E.: Recent Trends in SST, Chl-a, Productivity and Wind Stress in Upwelling and  
512 Open Ocean Areas in the Upper Eastern North Atlantic Subtropical Gyre, *J Geophys Res Oceans*, 126, e2021JC017268,  
513 <https://doi.org/10.1029/2021JC017268>, 2021.
- 514 Signorini, S. R., Franz, B. A., and McClain, C. R.: Chlorophyll variability in the oligotrophic gyres: Mechanisms, seasonality  
515 and trends, *Front Mar Sci*, 2, 1–11, <https://doi.org/10.3389/fmars.2015.00001>, 2015.
- 516 Smale, D. A. and Wernberg, T.: Satellite-derived SST data as a proxy for water temperature in nearshore benthic ecology, *Mar*  
517 *Ecol Prog Ser*, 387, 27–37, <https://doi.org/10.3354/MEPS08132>, 2009.
- 518 Sydeman, W. J., García-Reyes, M., Schoeman, D. S., Rykaczewski, R. R., Thompson, S. A., Black, B. A., and Bograd, S. J.:  
519 Climate change and wind intensification in coastal upwelling ecosystems, *Science* (1979), 345, 77–80,  
520 <https://doi.org/10.1126/science.1251635>, 2014.



521 Tel, E., Balbin, R., Cabanas, J. M., Garcia, M. J., Carmen Garcia-Martinez, M., Gonzalez-Pola, C., Lavin, A., Lopez-Jurado,  
522 J. L., Rodriguez, C., Ruiz-Villarreal, M., Sánchez-Leal, R. F., Vargas-Yáñez, M., and Vélez-Belchí, P.: IEOOS: The Spanish  
523 Institute of Oceanography Observing System, *Ocean Science*, 12, 345–353, <https://doi.org/10.5194/OS-12-345-2016>, 2016.  
524 Wang, D., Gouhier, T. C., Menge, B. A., and Ganguly, A. R.: Intensification and spatial homogenization of coastal upwelling  
525 under climate change, *Nature*, 518, 390–394, <https://doi.org/10.1038/nature14235>, 2015.  
526